Disorder induced band gap lowering in kesterite type $Cu_2ZnSnSe_4$ and $Ag_2ZnSnSe_4$: A *first-principles* and *special quasirandom structures* investigation

Daniel Fritsch[1, 2] and Susan Schorr[3, 4]

[1)]*Supercomputing Department, Zuse Institute Berlin, Takustr. 7, 14195 Berlin, Germany*[a)]

[2)]*Institute of Physics and Astronomy, University of Potsdam, Karl-Liebknecht-Str. 24/25, 14476 Potsdam, Germany*[b)]

[3)]*Department Structure and Dynamics of Energy Materials, Helmholtz-Zentrum Berlin für Materialien und Energie, Hahn-Meitner-Platz 1, 14109 Berlin, Germany*

[4)]*Institute of Geological Sciences, Freie Universität Berlin, Malteserstr. 74-100, 12249 Berlin, Germany*

(Dated: 5 September 2023)

Quaternary chalcogenides, i.e. Cu_2ZnSnS_4, crystallising in the kesterite crystal structure have already been demonstrated as potential building blocks of thin film solar cells, containing only abundant elements and exhibiting power conversion efficiencies of about 13 % so far. However, a correct determination of their ground state crystal structure has been hindered in the past by two structurally similar polymorphs, namely the kesterite and the stannite crystal structure. Additional complications arose from the later identified Cu-Zn disorder, present in virtually all thin film samples. Subsequently, is has been shown experimentally that this unavoidable Cu-Zn disorder leads to a band gap lowering in the respective samples. Additional theoretical investigations, mostly based on Monte-Carlo methods, tried to understand the atomistic origin of this disorder induced band gap lowering. Here, we present theoretical results from first-principles calculations based on density functional theory for the disorder induced band gap lowering in kesterite $Cu_2ZnSnSe_4$ and $Ag_2ZnSnSe_4$, where the Cu-Zn disorder is modelled via a supercell approach and special quasirandom structures. Results of subsequent analyses of structural, electronic, and optical properties will be discussed with respect to available experimental results, and will provide additional insight and knowledge towards the atomistic origin of the observed disorder induced band gap lowering in kesterite type materials.

One of the pillars of the third generation of solar cells rests upon thin films of quaternary chalcogenides crystallising in the kesterite crystal structure, already reaching power conversion efficiencies of about 13 %[1]. Most prominent examples comprise Cu_2ZnSnS_4 (CTZS), $Cu_2ZnSnSe_4$ (CZTSe), and their solid solution $Cu_2ZnSn(S_xSe_{1-x})_4$ (CZTSSe), with band gaps ranging from 1.0 eV[2,3] to 1.53 … 1.67 eV[4], thereby including the optimum band gap region of about 1.34 eV for single junction solar cells according to the Shockley-Queisser limit[5]. However, the actual device performance of such solar cells is limited by a large defect concentration of Cu-Zn antisite defects[6], e.g. Cu_{Zn}-Zn_{Cu} defect complexes due to Cu-Zn disorder[7], ultimately leading to a large deficit in the open-circuit voltage V_{oc}[8].

As a possible way to overcome this deficiency and to be more suitable for practical applications, a partial replacement of Cu in CZTSe with Ag has been proposed, shifting the focus towards $Ag_2ZnSnSe_4$ (AZTSe). In turn, investigations on the whole solid solution series have been performed, focusing on the structural and electronic properties[3,9].

All the quaternary chalcogenides of interest in the present work crystallise in the kesterite crystal structure (space group $I\bar{4}$, no. 82), which can be most easily visualised by starting from a doubled II-VI zincblende crystal structure and a subsequent application of two specific pairwise cation substitutions[10]. The resulting cation planes perpendicular to the crystallographic c-axis of the conventional ordered kesterite structure are shown in Fig. 1 (a), showing the Cu, Zn, and Sn cations at Wyckoff positions $(2a)(0,0,0)$ and $(2c)(0,\frac{1}{2},\frac{1}{4})$, $(2d)(0,\frac{1}{2},\frac{3}{4})$, and $(2b)(0,0,\frac{1}{2})$, respectively, while the Se anion are located at the general Wyckoff position $(8g)(x,y,z)$. However, a longstanding issue with kesterite type materials is the so-called Cu-Zn disorder, more or less pronounced in all grown samples depending on the growth conditions, and leading to a mixture of Cu and Zn cations within the Cu-Zn planes, thereby introducing additional symmetry elements as shown in Fig. 1 (b), and raising the symmetry to space group $I\bar{4}2m$ (no. 121). The fact that the disordered kesterite[11] and another possible chalcogenide polymorph, namely the stannite crystal structure, crystallise in the same space group ($I\bar{4}2m$, no. 121), has hindered the identification of a correct ground state crystal structure of these materials in the past[13].

Subsequently, there have been several attempts to understand the atomistic origin of the Cu-Zn disorder and its implications on the structural, electronic, and optical properties of kesterite type materials. On the experimental side, reports include a solid-state NMR and Raman spectroscopy study on CZTSSe by Paris *et al.*[14], a near-resonant Raman scattering investigation by Scragg *et al.*[15], neutron diffraction studies of CZTS by Schorr *et al.*[16] and Bosson *et al.*[17], and complementary neutron and anomalous X-ray diffraction studies by Többens *et al.*[18] and Gurieva *et al.*[19], respectively. These experimental studies are corroborated by theoretical investigations utilising a combination of first-principles calculations based on density functional theory (DFT) and Monte Carlo calculations based on cluster expansion methods[20–23].

[a)]Electronic mail: fritsch@zib.de

[b)]Electronic mail: daniel.fritsch@uni-potsdam.de

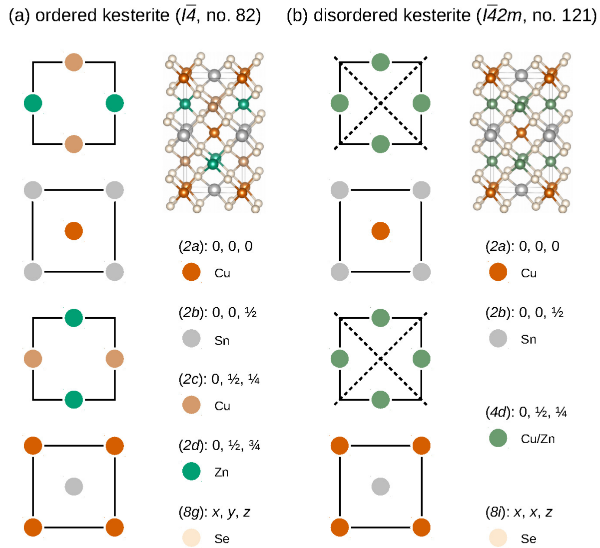

FIG. 1. Cu, Zn, and Sn cation planes with $z = 0.0, 0.25, 0.5$ and 0.75 (bottom to top) in the (a) ordered kesterite (space group $I\bar{4}$, no. 82) and (b) disordered kesterite[11] (space group $I\bar{4}2m$, no. 121) crystal structures, respectively. The dashed lines in the disordered kesterite structure (b) denote additional symmetry elements due to the total Cu-Zn disorder in the $z = 0.25$ and $z = 0.75$ planes. Also given are the colour-coded Wyckoff positions for each of the structural polymorphs. The crystal structure figures have been prepared using VESTA[12].

In general, any deviation from perfect crystallinity poses additional complications for an accurate theoretical description. With limited access to describe partial occupancies of Wyckoff positions, one method of choice relies on the calculation of bulk structural properties utilising first-principles calculations based on DFT and a subsequent cluster expansion model calculation based on Monte Carlo methods[20–23]. However, from the need to accurately describe binary $A_{1-x}B_x$ alloys with first-principles methods, a different approach based on *special quasirandom structures* has been developed by Zunger *et al.*[24]. Therein, after choosing a suitable supercell size, all possible populations over the alloy site are generated, and after additional application of crystalline symmetry, the total number of strictly necessary cation distributions gets reduced by only taking into account symmetry inequivalent ones. Over the years, several program packages have been developed for that purpose[25–27].

Here, we model the Cu-Zn disorder in CZTSe and AZTSe based on these *special quasirandom structures*. Starting points of our investigation are the ground state properties of CZTSe and AZTSe which have been investigated previously using a range of exchange and correlation functionals[13]. Utilising the SCAN exchange and correlation functional[28], the lattice parameters of the conventional kesterite unit cell showing full cation order amount to a=5.695 Å and c=11.340 Å (a=6.072 Å and c=11.362 Å) for CZTSe (AZTSe), respectively, in very good agreement with the experimental results of a=5.693 Å and c=11.347 Å (a=6.046 Å and c11.340 Å) obtained from a recent combined neutron and X-ray diffraction study on powder samples by Gurieva *et al.*[3]. Based on the mentioned ground state lattice constants, we generate $2\times1\times1$ supercells of the conventional kesterite unit cell, each containing four formula units (32 atoms). More importantly, we now have four Cu (Ag) and four Zn cations occupying the (2c) and (2d) Wyckoff positions of the ordered kesterite structure, or equivalently the (4d) Wyckoff position in the disordered kesterite structure (Fig. 1). For the generation of the *special quasirandom structures* we rely on the supercell program of Okhotnikov *et al.*[27], which reduces the original $\binom{8}{4} = 70$ different possible cation arrangements for the Cu-Zn disorder to just ten symmetry-inequivalent cation distributions by applying symmetry constraints. Exemplary, these ten symmetry-inequivalent cation distributions are shown for CZTSe in Fig. 2. It should be noted that an earlier investigation where the Cu and Zn cations were distributed over the (2c) and (2d) Wyckoff positions with no mixing allowed, resulted in only seven symmetry-inequivalent cation distributions to describe the Cu-Zn disorder in CZTSe[10].

Similarly to our earlier work[13], all the calculations of the present work have been performed utilising the Vienna *ab initio* Simulations package (VASP 5.4.4)[29–31] together with the projector-augmented wave (PAW) method[32,33]. The calculations employed the recommended PAW potentials supplied by VASP that contributed 17, 17, 12, 14, and 6 valence electrons for the Cu, Ag, Zn, Sn, and Se atoms, respectively. In order to understand possible influences of the Cu-Zn disorder on the structural properties, we performed full structural relaxations for each of the ten different cation distributions for CZTSe and AZTSe. Besides a k-point grid of $4\times8\times4$, a cut-off energy of the plane-wave expansion of 500 eV and a convergence criteria for the total energy of 10^{-6} eV ensured well-converged results.

For each of the ten different cation distributions for CZTSe and AZTSe we have calculated the total energy curves taking into account several volumes around the previously determined ordered kesterite ground state volumes. While we kept the different unit cell volumes fixed during the structural optimisations, all the internal coordinates have been allowed to relax until the forces on the atoms were below 0.001 eVÅ^{-1}. A subsequent analysis using Murnaghan's equation of state[34,35]

$$E(V) = E(V_0) + \frac{B_0 V}{B_0'}\left[\frac{(V_0/V)^{B_0'}}{B_0' - 1} + 1\right] - \frac{V_0 B_0}{B_0' - 1} \qquad (1)$$

yielded the ground state volumes of each of the ten different cation distributions. The resulting total energy curves are shown as grey lines in the middle panels of Fig. 2 for CZTSe (left) and AZTSe (right), with the lowest total energy set to zero and normalised to one formula unit (f.u.), respectively.

Immediately, one recognises the large spread in total energy over the ten different cation distributions, reaching 190 meV (254 meV) per f.u. for CZTSe (AZTSe) between the lowest and highest energy solution. However, in order to correctly describe the disordered kesterite crystal structures, a weighted average over the ten different cation distributions has to be performed, resulting in the total energy curves shown as dashed green lines in the middle panels of Fig. 2. For com-

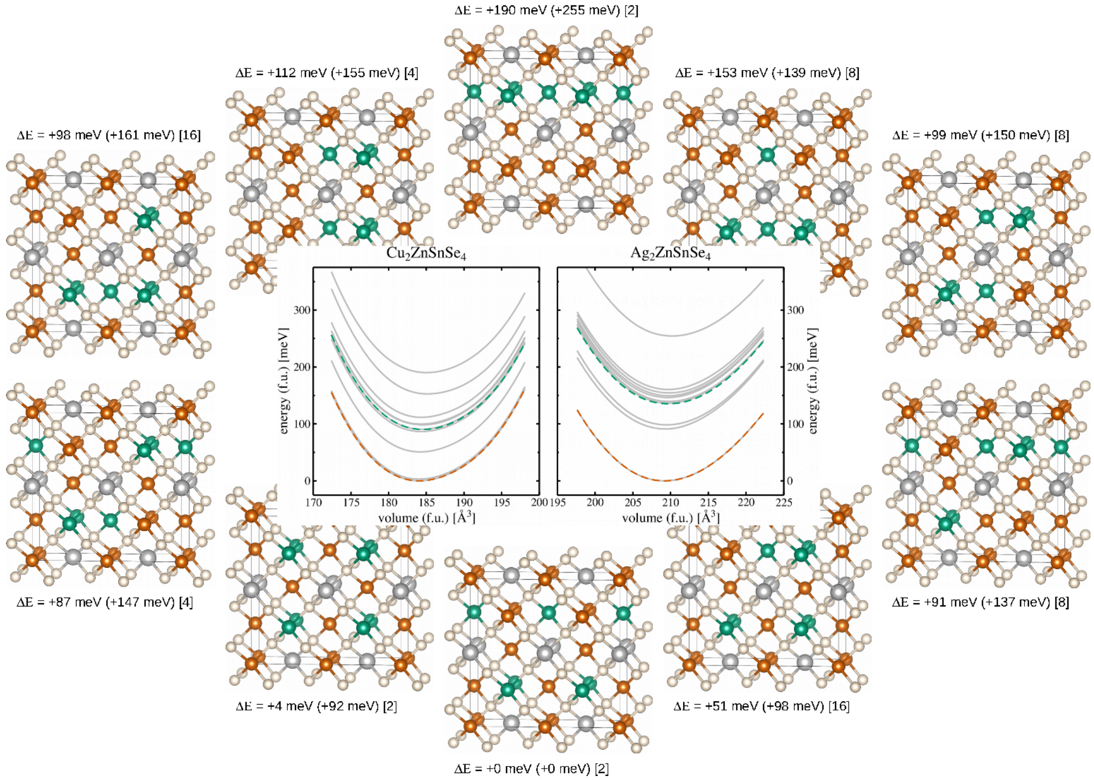

FIG. 2. $2\times1\times1$ supercells depicting the ten symmetry inequivalent cation distributions of Cu (orange) and Zn (green) over the (2c) and (2d) Wyckoff positions as generated by the supercell program[27]. The lowest supercell depicts the ordered kesterite crystal structure, and the total energy differences ΔE are given in meV and per formula unit for CZTSe (AZTSe) including the respective degeneracy of the supercell in square brackets. Structural optimisation by means of the SCAN exchange and correlation functional of each of these supercells yielded their respective total energy curves, as shown in the middle figures, where the grey lines correspond to the ten symmetry inequivalent cation distributions, the dashed green lines are their weighted averages, and the dashed red lines show the results from the ordered kesterite crystal structures for comparison. The crystal structure figures have been prepared using VESTA[12].

parison, the total energy curves of the ordered kesterite crystal structures are shown as dashed red lines, resulting in an energy difference between the ordered and disordered kesterite structures of 90 meV (135 meV) per f.u. for CZTSe (AZTSe). These results show that the ordered kesterite crystal structure is the thermodynamically stable crystal structure at zero temperature of the DFT calculations. The disordered kesterite crystal structure is then due to temperature effects and growth conditions of experimentally investigated samples[15].

What's less obvious from the weighted average total energy curves for the disordered kesterite crystal structures is the change towards larger unit cell volumes compared to the ordered kesterite crystal structures by approximately 0.2 %. This is in line with an experimental investigation on the temperature dependency of Cu-Zn disorder in CZTSe by Többens *et al.*[18] and theoretical predictions[36]. In addition, we further analysed the ground state crystal structures of each of the ten different cation distributions for CZTSe and AZTSe. We employed VESTA[12] to obtain X-ray diffraction patterns for each of the cation distributions, and again performed a weighted average in case of the disordered kesterite structures. The obtained X-ray diffraction patterns for the ordered kesterite (black lines) and the disordered kesterite crystal structures (red lines) are shown in the upper panels of Fig. 3 for CZTSe (a) and AZTSe (b), respectively.

While the difference between the X-ray diffraction patterns between the ordered and disordered kesterite crystal structures seems to be negligible for CZTSe, there are additional peaks clearly visible for the disordered kesterite crystal structure of AZTSe. This interesting finding might explain why Ag substitution into CZTSe has such a positive effect on the performance of actual solar cell devices. To further this idea, a detailed investigation into the structural properties of Ag substituted CZTSe would have to be performed, similar to the approach taken in the present work. However, here we are limited to the investigation of the effect of Cu-Zn (Ag-Zn) disorder in CZTSe (AZTSe), and might keep the respective calculations and analyses in mind for future investigations.

A subsequent pair distribution function analysis employing the R.I.N.G.S code[37] gave access to the bond distances, shown for the selected Cu-Cu (Ag-Ag), Zn-Zn, Cu-Se (Ag-Se), and Zn-Se bonds for CZTSe (AZTSe) in the lower panels of Fig. 3, respectively. As can be seen, the bond distances for the disordered kesterites are broadened compared to the ordered kesterite crystal structures, reflecting the slightly larger unit cell volumes. In addition, especially the first nearest

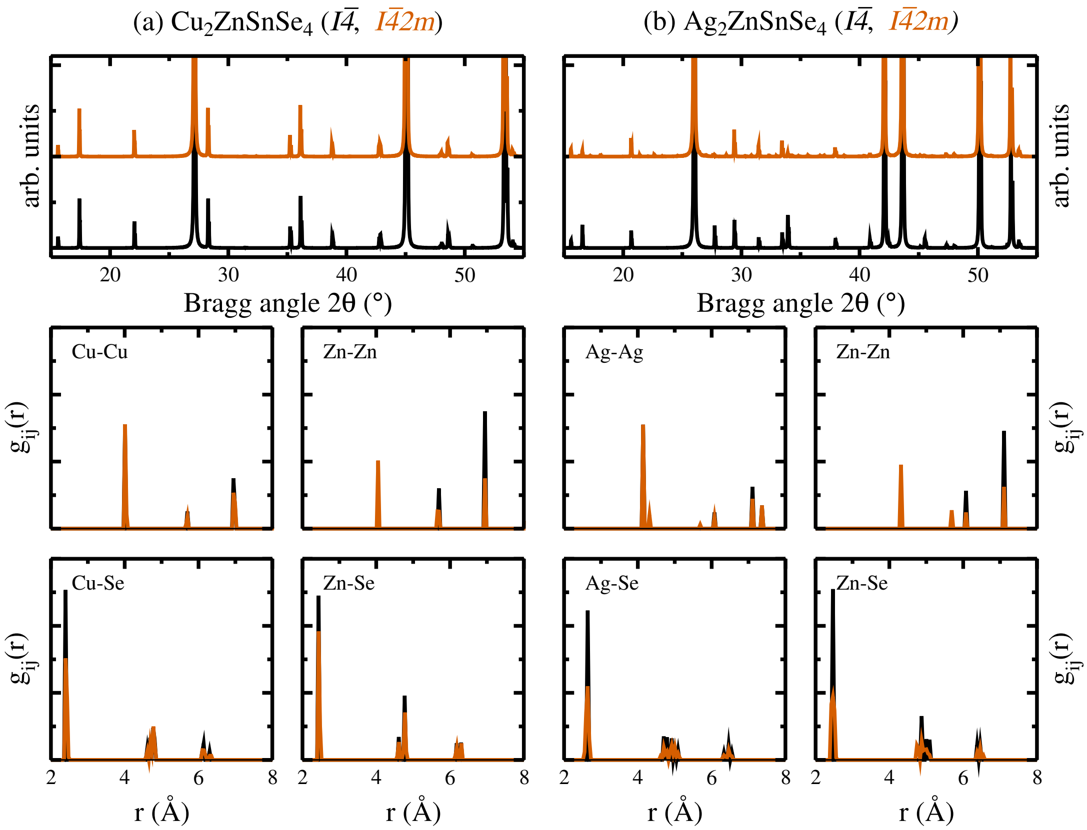

FIG. 3. Upper panels: X-ray diffraction pattern for the ordered (black lines) and disordered kesterite crystal structures (red lines) for (a) CZTSe and (b) AZTSe obtained from a pair distribution function analysis employing the R.I.N.G.S code[37]. Lower panels: Selected bond distances for (a) CZTSe and (b) AZTSe, again for the ordered (black lines) and disordered kesterite crystal structures (red lines).

neighbour cation-Se bond distances are reduced in intensity, highlighting the reduction of the specific cation-Se pairs due to disorder.

Apart from the effect of the Cu-Zn (Ag-Zn) disorder in CZTSe (AZTSe) on the structural properties and the observed slight increase in unit cell volumes, we're particularly interested in the influence on the electronic properties. It has been shown for the bulk crystal structures of CZTSe and AZTSe that calculations based on the SCAN exchange and correlation functional severely underestimate the band gap[10,13]. To partly correct for this we performed single-shot calculations employing the hybrid exchange and correlation functional HSE06[38], thereby keeping the previously determined ground state crystal structures of symmetry inequivalent cation distributions of CZTSe and AZTSe fixed. Again, calculating the density of states (DOSs) for each of the ten different cation distributions for CZTSe and AZTSe and performing the weighted averages, gave access to the DOSs for the disordered kesterite crystal structures as shown in the lower panels of Fig. 4 for CZTSe (a) and AZTSe (b), respectively.

In comparison, the upper panels of Fig. 4 show the DOSs for the ordered kesterite crystal structures. In all panels the shaded grey background depicts the total DOS, whereas the red, green, and black solid lines show the partial DOSs belonging to Cu (4d), Se (8i), and Sn (2b) atoms, respectively. Three main results are immediately visible from the comparison of the upper and lower panels comparing the DOSs of the ordered and disordered kesterite crystal structures: (1) the DOSs for the disordered kesterites are smoother compared to the ordered kesterites, but their overall values are similar; (2) the partial DOSs at the valence band maxima and conduction band minima consist of the same contributions, i.e. there is no change in orbital character at the band edges, and (3) the conduction band minima of the disordered kesterites are shifted towards smaller energies compared to the ordered kesterites, resulting in a band gap lowering of about 182 meV and 208 meV for CZTSe and AZTSe, respectively.

Lastly, based on the obtained ground state crystal structures for the various cation distributions we also calculated the optical properties, i.e. the real and imaginary parts of the dielectric functions and absorption coefficients, as described in more detail in some earlier works[39,40]. Again, for the disordered kesterites we performed a weighted average, resulting in absorption coefficients for the disordered (red lines) and ordered kesterite crystal structures (black lines), as shown in Fig. 5 for CZTSe (a) and AZTSe (b).

Similarly to the structural properties we recognise a smoothening of the curves for the disordered kesterites and a clearly visible shift of the onset in the absorption towards lower energies, indicating the already observed band gap low-

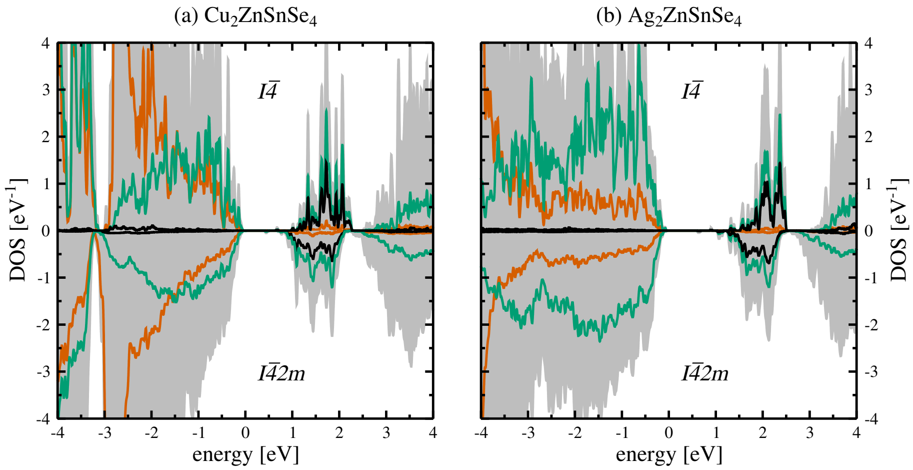

FIG. 4. Densities of states (DOSs) for (a) CZTSe and (b) AZTSe, calculated by means of the HSE06 exchange and correlation functional. Upper (lower) panels show the respective DOSs for the ordered (space group $I\bar{4}$) and the disordered (space group $I\bar{4}2m$) kesterite crystal structures. While the shaded grey backgrounds show the total DOSs, the red, green, and black solid lines depict the partial DOSs belonging to Cu (4d), Se (8i), and Sn (2b) atoms, respectively. The valence band maximum is set to zero energy in all panels.

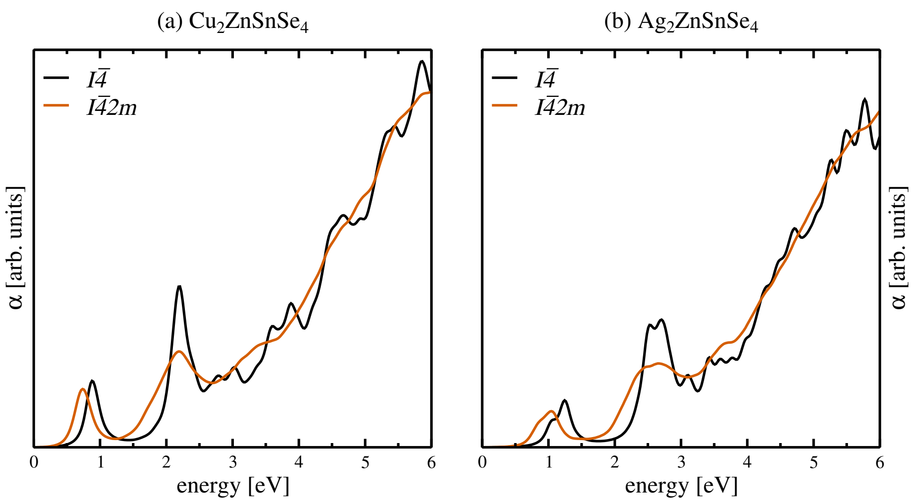

FIG. 5. Absorption coefficients for (a) CZTSe and (b) AZTSe. Shown are the results for the disordered (red lines) and ordered (black lines) kesterite crystal structures.

ering due to Cu-Zn (Ag-Zn) disorder in CZTSe (AZTSe), respectively.

In summary, we applied hitherto not employed *special quasirandom structures* to describe the influence of Cu-Zn (Ag-Zn) disorder on the structural, electronic, and optical properties of CZTSe (AZTSe). We confirmed the experimental finding of slightly increased unit cell volumes for the disordered kesterites, and provided a detailed analysis comparing the generated X-ray diffraction pattern and bond distributions for the ordered and disordered kesterite crystal structures of CZTSe and AZTSe. Single-shot hybrid functional calculations allowed for a better description of electronic properties, namely the total and partial DOSs and band gap energies, revealing an unchanged orbital character of partial DOSs at the valence band maxima and conduction band minima for CZTSe and AZTSe, respectively, and a band gap lowering due to the Cu-Zn (Ag-Zn) disorder in CZTSe (AZTSe). Finally, the disorder induced band gap lowering is also clearly visible in the calculated absorption coefficients, comparing the ordered kesterite crystal structures with the disordered ones.

ACKNOWLEDGMENTS

This work made use of computational resources provided by the North-German Supercomputing Alliance (HLRN, www.hlrn.de), and the ZEDAT[41] and DIRAC high-performance computing facilities of the Freie Universität Berlin and the Helmholtz-Zentrum Berlin, respectively.

[1] NIST Best research-cell efficiency chart, https://www.nrel.gov/pv/cell-efficiency.html, accessed: 2021-10-25.

[2] S. Siebentritt and S. Schorr, Prog. Photovolt: Res. Appl. **20**, 512 (2012).

[3] G. Gurieva, J. A. Márquez, A. Franz, C. J. Hages, S. Levcenko, T. Unold, and S. Schorr, Phys. Rev. Mater. **4**, 054602 (2020).
[4] S. Levcenko, E. Hajdeu-Chicarosh, E. Garcia-Llamas, R. Caballero, R. Serna, I. V. Bodnar, I. A. Victorov, M. Guc, J. M. Merino, A. Pérez-Rodriguez, E. Arushanov, and M. León, Appl. Phys. Lett. **112**, 161901 (2018).
[5] S. Rühle, Solar Energy **130**, 139 (2016).
[6] S. Chen, A. Walsh, X.-G. Gong, and S.-H. Wei, Adv. Mater. **25**, 1522 (2013).
[7] S. Bourdais, C. Choné, B. Delatouche, A. Jacob, G. Larramona, C. Moisan, A. Lafond, F. Donatini, G. Rey, S. Siebentritt, A. Walsh, and G. Dennler, Adv. Energy Mater. **6**, 1502276 (2016).
[8] Z.-K. Yuan, S. Chen, H. Xiang, X.-G. Gong, A. Walsh, J.-S. Park, I. Repins, and S.-H. Wei, Adv. Funct. Mater. **25**, 6733 (2015).
[9] D. Fritsch and S. Schorr, Thin Solid Films **NA**, NA (2021).
[10] D. Fritsch, Crystallographic diffraction techniques and density functional theory: two sides of the same coin?, in *Crystallography in Materials Science*, edited by S. Schorr and C. Weidenthaler (De Gruyter, 2021) p. 317.
[11] M. Y. Valakh, V. M. Dzhagan, I. S. Babichuk, X. Fontane, A. Perez-Rodriquez, and S. Schorr, JETP Lett. **98**, 255 (2013).
[12] K. Momma and F. Izumi, J. Appl. Crystallogr. **44**, 1272 (2011).
[13] D. Fritsch and S. Schorr, J. Phys. Energy **3**, 015002 (2021).
[14] M. Paris, L. Choubrac, A. Lafond, C. Guillot-Deudon, and S. Jobic, Inorg. Chem. **53**, 8646 (2014).
[15] J. J. S. Scragg, L. Choubrac, A. Lafond, T. Ericson, and C. Platzer-Björkman, Appl. Phys. Lett. **104**, 041911 (2014).
[16] S. Schorr, H.-J. Hoebler, and M. Tovar, Eur. J. Mineral. **19**, 65 (2007).
[17] C. J. Bosson, M. T. Birch, D. P. Halliday, K. S. Knight, A. S. Gibbs, and P. D. Hatton, J. Mater. Chem. **5**, 16672 (2017).
[18] D. M. Többens, G. Gurieva, S. Levcenko, T. Unold, and S. Schorr, Phys. Status Solidi B **253**, 1890 (2016).
[19] G. Gurieva, D. M. Többens, S. Levcenco, T. Unold, and S. Schorr, J. Alloys Comp. **846**, 156304 (2020).
[20] K. Yu and E. A. Carter, Chem. Mater. **28**, 864 (2016).
[21] S. P. Ramkumar, A. Miglio, M. J. van Setten, D. Waroquiers, G. Hautier, and G.-M. Rignanese, Phys. Rev. Mater. **2**, 085403 (2018).
[22] S. K. Wallace, J. M. Frost, and A. Walsh, J. Mater. Chem. A **7**, 312 (2019).
[23] Y.-F. Zheng, J.-H. Yang, and X.-G. Gong, AIP Advances **9**, 035248 (2019).
[24] A. Zunger, S.-H. Wei, L. G. Ferreira, and J. E. Bernard, Phys. Rev. Lett. **65**, 353 (1990).
[25] R. Grau-Crespo, S. Hamad, C. R. A. Catlow, and N. H. de Leeuw, J. Phys.: Condens. Matter **19**, 256201 (2007).
[26] S. Mustapha, P. D'Arco, M. De La Pierre, Y. Noël, M. Ferrabone, and R. Dovesi, J. Phys.: Condens. Matter **25**, 105401 (2013).
[27] K. Okhotnikov, T. Charpentier, and S. Cadars, J. Cheminform. **8**, 17 (2016).
[28] J. Sun, A. Ruzsinszky, and J. P. Perdew, Phys. Rev. Lett. **115**, 036402 (2015).
[29] G. Kresse and J. Hafner, Phys. Rev. B **47**, 558 (1993).
[30] G. Kresse and J. Hafner, Phys. Rev. B **49**, 14251 (1994).
[31] G. Kresse and J. Furthmüller, Comp. Mat. Sci. **6**, 15 (1996).
[32] P. E. Blöchl, Phys. Rev. B **50**, 17953 (1994).
[33] G. Kresse and D. Joubert, Phys. Rev. B **59**, 1758 (1999).
[34] F. D. Murnaghan, Amer. Jour. Math. **59**, 235 (1937).
[35] F. D. Murnaghan, PNAS **30**, 244 (1944).
[36] S. Chen, X. G. Gong, A. Walsh, and S.-H. Wei, Appl. Phys. Lett. **94**, 041903 (2009).
[37] S. Le Roux and P. Jund, Comp. Mat. Sci. **49**, 70 (2010).
[38] J. Heyd, G. E. Scuseria, and M. Ernzerhof, J. Chem. Phys. **118**, 8207 (2003), *erratum*: 2006 *J. Chem. Phys.* **124** 219906.
[39] D. Fritsch, Advances in Materials Science and Engineering **vol. 2018**, Article ID 6416057 (2018).
[40] D. Fritsch, Phys. Status Solidi A **215**, 1800071 (2018).
[41] L. Bennett, B. Melchers, and B. Proppe, Curta: A general-purpose high-performance computer at ZEDAT, Freie Universität Berlin (2020).